Adjustable Hyperthermia Response of Self-Assembled Ferromagnetic Fe-MgO Core–Shell Nanoparticles by Tuning Dipole–Dipole Interactions

*Carlos Martinez-Boubeta, Konstantinos Simeonidis, David Serantes, Iván Conde-Leborán, Ioannis Kazakis, George Stefanou, Luis Peña, Regina Galceran, Lluis Balcells, Claude Monty, Daniel Baldomir, Manassis Mitrakas, and Makis Angelakeris**

The Fe-MgO core-shell morphology is proposed within the single-domain nanoparticle regime as an enhanced magnetically driven hyperthermia carrier. The combinatory use of metallic iron as a core material together with the increased particle size (37–65 nm) triggers the tuning of dipolar interactions between particles and allows for further enhancement of their collective heating efficiency via concentration control. A theoretical universal estimation of hysteresis losses reveals the role of dipolar interactions on heating efficiency and outlines the strong influence of coupling effects on hyperthermia opening a novel roadmap towards multifunctional heat-triggered theranostics particles.

Dr. C. Martinez-Boubeta
Departament d'Electrònica
MIND-IN2UB, Universitat de Barcelona
Barcelona 08028, Spain

Dr. K. Simeonidis
Department of Mechanical Engineering
School of Engineering
University of Thessaly
Volos 38334, Greece

Dr. D. Serantes, Dr. I. Conde-Leborán, Dr. D. Baldomir
Instituto de Investigacións Tecnolóxicas
and Departamento de Física Aplicada
Universidade de Santiago de Compostela
Santiago de Compostela 15782, Spain

I. Kazakis, G. Stefanou, Prof. M. Angelakeris
Department of Physics
Aristotle University of Thessaloniki
Thessaloniki 54124, Greece
E-mail: agelaker@auth.gr

L. Peña, R. Galceran, Dr. L. Balcells
Institut de Ciència de Materials de Barcelona, Campus Universitat
Autònoma de Barcelona, Bellaterra 08193, Spain

Dr. C. Monty
Procédés, Matériaux et Energie Solaire
Centre National de la Recherche Scientifique
Odeillo, Font-Romeu 66120, France

Prof. M. Mitrakas
Analytical Chemistry Laboratory
Department of Chemical Engineering
Aristotle University of Thessaloniki
Thessaloniki 54124, Greece

DOI: 10.1002/adfm.201200307

1. Introduction

Biocompatible magnetic nanoparticles have emerged as important materials in biomedical research, capable for example, of the diagnosis, imaging and selective destruction of tumors.[1,2] Indeed, the same magnetic entities may serve as a contrast agent for magnetic resonance imaging (MRI) and also as a heating dissipation center for hyperthermia.[3,4] Under this framework, most experimental studies so far have explored superparamagnetic (SPM) particles of iron oxide-based nanostructures. Currently, a large effort is being devoted to the enhancement of magnetic imaging contrast and heating efficacy of particles by tuning the magnetic profile (i.e size, anisotropy constant, saturation magnetization).[5,6] In this aspect, metallic iron appears as a promising candidate since its bulk magnetic moment is more than double of the corresponding one for Fe_3O_4, though its high reactivity is an obstacle for both its stabilization in nanoparticle form and its applicability in biological environment. An additional synthetic step may be considered if the particle is artificially modulated to achieve a core-shell structure, which not only provides oxidation resistance to the magnetic core but might also help to confront the toxicity issue, as well. The shell proposed here, i.e. MgO is based on magnesium, an exceptionally lightweight metal, essential to human metabolism that is naturally found in bone tissue and is the fourth most abundant cation in the human body and a co-factor for many enzymes, also stabilizing the structures of DNA and RNA. Whereas a huge number of methods have been developed for the scalable synthesis and preparation of inorganic metal and semiconductor nanoparticles, only a few specialized methodologies have been reported for the preparation of core-shell magnetic nanoparticles.[7,8]

On the other hand, the dipolar interactions between adjacent particles favor their assembly into chains, as observed in the case of natural origin magnetosomes,[9] and even for SPM lab synthesized nanoparticles.[10,11] It has been shown that such elongated assemblies of nanoparticles both improve the blood circulation half-life and MRI contrast, which facilitates efficient drug-delivery and enhances the resolution in medical imaging,[12] being also capable of delivering large heating

power.[13] But in the transitional region between SPM and blocked magnetic particles, difficulties with dipolar coupling effects, due to neighboring particles, and the interpretation of magnetic loss measurements may arise,[14] since the frequency-dependent collective behavior of nanoparticles shows large differences compared to that of isolated particles.[15] There are theoretical models in the literature predicting that hyperthermia's specific loss power (SLP) depends on the particle's magneto-structural properties such as mean diameter, size distribution, magnetic moment per particle and anisotropy, as well as on the viscosity of the medium in which they are dispersed, the amplitude and the frequency of the alternating applied field.[16] Therefore, with the progress in controlling the aforementioned parameters, increasingly large values of SLP have been reported along the last years.[5] Note that within these models the SLP does not depend on concentration.[17,18] Specifically, mainly SPM particles and their heating efficiencies have been systematically investigated since larger particles, residing in multidomain regions, were found to exhibit considerably lower hysteresis loss heating efficiency when compared with smaller SPM.[6,19]

Here we show that multifunctional core–shell nanoparticles consisting of a single-domain metallic Fe core covered with a biocompatible MgO shell can attain a significant increase in the efficiency of magnetic thermal induction compared to conventional superparamagnetic oxides due to interparticle dipolar interactions' substantial influence. In vivo analysis revealed that these Fe-MgO nanostructures satisfy demands for biocompatibility and non-toxicity,[3] while further investigation of their uptake in breast cancer cells and their heating ability under ac magnetic field verified their potential for efficient and fast hyperthermia treatment.[20] As an extension of previous work on epitaxial Fe-MgO core-shell nanostructures,[3,18,21] the current study examines the synthetic conditions-parameters that determine the final size of particles produced by solar physical vapor deposition and evaluates their efficiency as magnetic hyperthermia agents. In this regard, we will focus on spherical particles with a diameter around ~50 nm, the optimal size for internalization into mammalian cells,[22] which provides a valuable piece of information for the rational design of magnetic-based anticancer delivery protocols, especially when considering intracellular hyperthermia.[23] Results demonstrate values above 1 kW/g at 765 kHz and 300 Oe, among the highest specific losses reported in the literature so far. Furthermore, a novel universal theoretical dependence of the hyperthermia response based on correlation of the magneto-structural properties with particle concentration is presented. These findings may have important clinical implications in cancer treatment.

Our methodology for the fabrication of core-shell nanoparticles is schematically illustrated in **Figure 1**. Briefly, the high-moment nanoparticles were synthesized directly from the gas phase by using a physical vapor deposition technique under inert argon atmosphere. This process has been developed at PROMES facilities in Odeillo-Font Romeu (France) using reactors operating with concentrated sunlight in a solar furnace apparatus. The solar furnace is constituted of a mobile plane mirror which tracks the sun and reflects the radiation on a 2 kW parabolic concentrator (Ø 2 m).

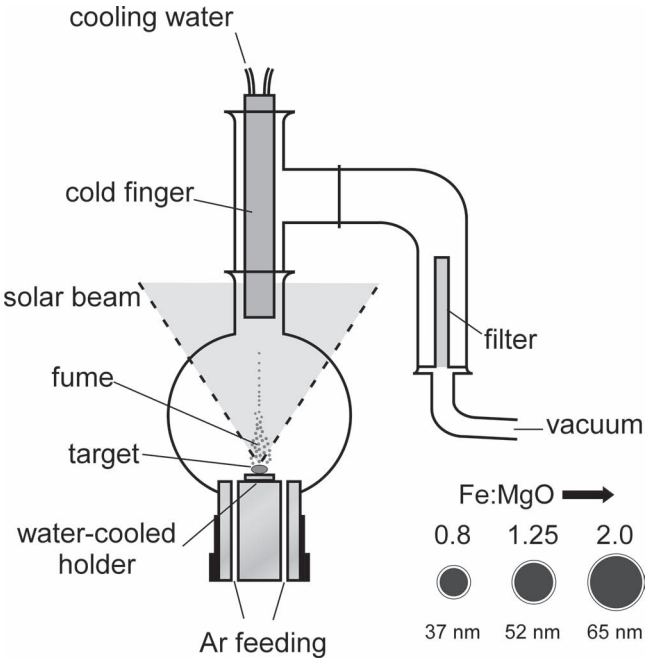

Figure 1. Schematic representation of the solar physical vapor deposition arrangement used for the growth of Fe-MgO nanoparticles.

The target-material to be melted is placed onto a water-cooled holder in the center of a glass vacuum chamber. The chamber's pressure, adjusted in the high vacuum region by introducing argon, is maintained by a rotary pump. The target is transferred to the focus of the concentrator and evaporation starts to take place. Shields facilitate the growth rate control by regulating the solar beam. Particles are collected in a cold finger (nanoporous ceramic filter). By this setup, the nanoparticle production rate is about 1 g/h when the beam flux is in the order of 1 kW/m^2. The control of the Fe-to-MgO evaporation ratio and the final particle size was achieved by the variation of the iron-to-magnesium ratio. Aiming towards a hyperthermia nanoparticle carrier with magnetic properties such as anisotropy constant and M_S close to the bulk values, we limited ourselves to targets with Fe proportions up to 60% wt. For higher Fe percentage, the MgO surrounding shell quantity was not sufficient to completely cover the Fe nuclei, which were then susceptible to oxidation as reported elsewhere.[24] Specifically, the iron content in the corresponding targets was 40, 50 and 60% wt., while Mg content was 10% wt. and the rest was MgO. This high-energy and high throughput methodology may produce nanopowders (chemical analysis of produced nanoparticles: Fe wt. 35, 50, 70%) of Fe composition similar to corresponding targets (Fe wt. 40, 50, 60%) despite the fact that the vapor pressures of Fe, MgO and Mg are not equal potential reason for differences in composition between target mixtures and final products. Since the chamber's pressure and the beam energy were similar for all sample preparations, the final size, and more specifically the diameter of Fe core and the thickness of MgO shell, was ultimately determined by the Fe-to-MgO mass ratio in the target. Probably, surface diffusion is the key factor in determining material transport and therefore growth modes while

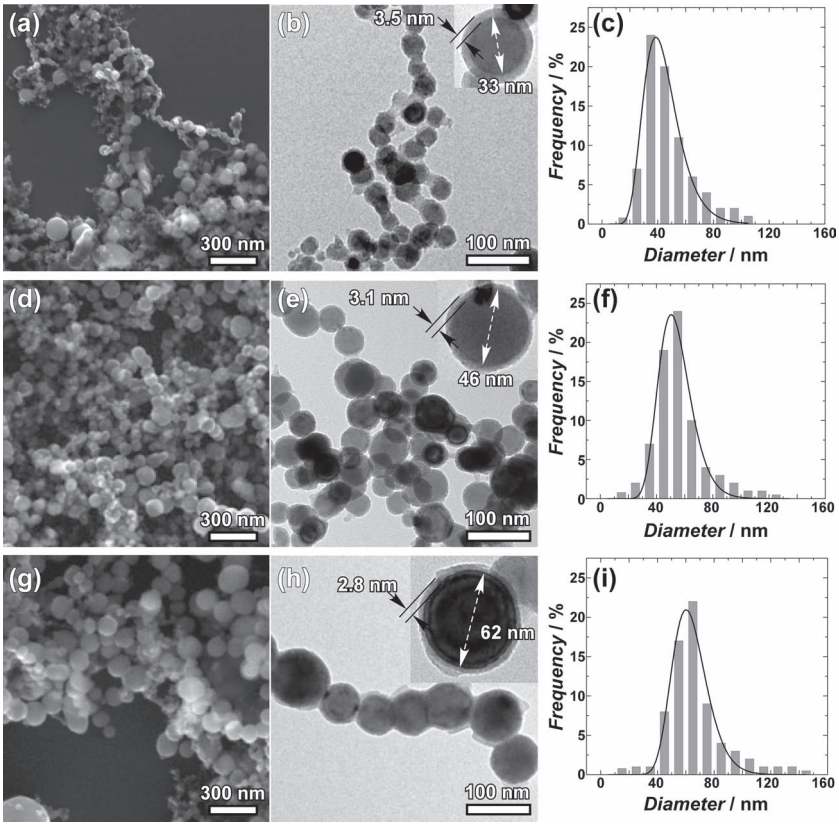

Figure 2. Sample 1: 37 nm (a–c), Sample 2: 52 nm (d–f) and Sample 3: 65 nm (g–i). SEM images (a), (d), (g) and log-normal size distributions of Fe-MgO nanoparticle samples (c), (f), (h). Corresponding high magnification TEM images illustrating the particles arrangement and their core-shell configuration (b), (d), (h). Insets depict HREM core/shell morphology.

the MgO self-assembles on the Fe surface because of differences in surface energy (2900 nJ/mm^2 for Fe and 1200 nJ/mm^2 for MgO), interfacial stress probably modifies the radial growth of the shell and limits the MgO thickness.

The existence of MgO shell for the protection of the magnetic core against oxidation in air is initially verified from the crystallographic investigation of the nanoparticles performed by X-ray diffraction (XRD) (see the Supporting Information, S.1 section). The samples are mainly consisting of bcc-iron and MgO whereas Mg is also identified due to the excess of Mg used during evaporation. Results were quantified by fitting the XRD data with the application of Rietveld method in the FullProf software,[25] on the basis of cubic Fe (space group: Im-3m), fcc MgO (space group: Fm-3m) and hexagonal Mg (space group: P63-mmc). Combining the results of the quantitative structural determination (shown in the Supporting Information, S.1 section), the chemical analysis and the initial target's composition, it is concluded that a linear correlation is achieved in the composition of the target and the product under the vaporization-condensation conditions described.

Figure 2 presents the scanning electron microscope (SEM) images of large areas of the three samples and the derived size distributions of the observed nanoparticles fitted by a log-normal function.

The average nanoparticle diameter was measured to be 37, 52 and 65 nm for samples 1, 2 and 3, respectively. Standard deviation was around 15–20% in all cases.

A more detailed view of the morphological characteristics of the nanoparticles is obtained by the transmission electron microscopy (TEM) images is also depicted in Figure 2. In general, particles appear to be isolated without serious agglomeration effects despite their relatively large diameter. Nevertheless, dipole-dipole magnetic interactions favor the formation of linear particle arrangements, which are more obvious in sample 3 (Figure 2(h)). The successful coating of nanoparticles by MgO and the shell thickness were verified by higher magnification images focused on separate nanoparticles (insets of Figure 2(b), (e), (h)). It is concluded that the smaller the particles the better the MgO coverage since shell thickness varies between 3.5 nm for smaller particles (Sample 1 with mean diameter of 37 nm) and gradually reduces to less than 3 nm in samples with higher diameters (3.1 nm for sample 2 with mean diameter of 52 nm and 2.8 nm for sample 3 with mean diameter of 65 nm). The thickness variation of the MgO capping layer could also modify the interparticle distances and interactions, which are also expected to play an important role in determining the hyperthermia output and colloidal stability.

Although for parenteral administration long-term stability is not of high priority, the colloidal stability of the dispersions may affect their efficacy during the ac-field hyperthermia experiments. Since, TEM imaging provides no direct proof for the actual agglomeration state of particles in the liquid phase[10] it was essential to examine the surface charge over the expected pH range of use. **Figure 3** presents the zeta potential variation of the three samples dispersed in water adjusted at pH 6–13.8. The isoelectric point in all cases was found to be above 11.5, very close to the expected value for MgO.[26] On the one hand, this result supports the existence of the MgO coating of nanoparticles which is the determining compound of the surface charge. In addition, the fact that zeta potential of nanoparticles remains above +20 mV in the pH range of practical interest <8, guarantees that the particles are sufficiently charged to maintain stability of the corresponding dispersions while agglomeration and sedimentation are hindered due to electrostatic repulsions.

Magnetic measurements (**Figure 4**) revealed that nanoparticles appear to be ferromagnetic at room temperature. The saturation magnetization of the samples (from 80 to 150 emu/g) scales with the Fe content. Once the iron content within each powder is taken into account, the saturation magnetization values roughly reach that of bulk bcc iron,[3] further confirming the magnetic properties of the nanoparticle samples described here are very similar. Noteworthy, the transition from single-domain to multi-domain configuration for Fe particles has been

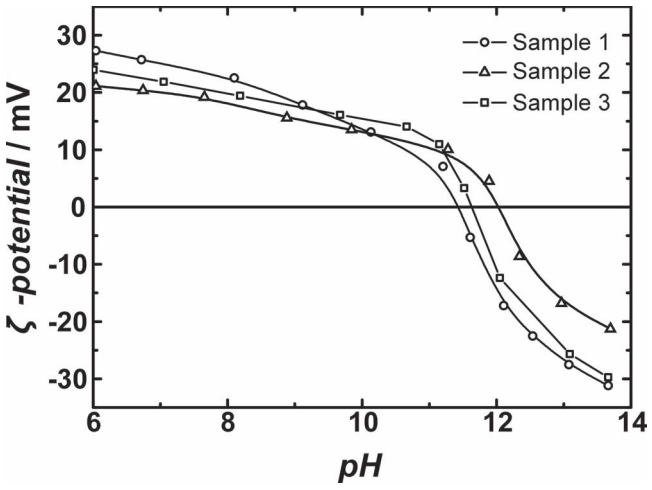

Figure 3. Zeta potential variation versus solution pH for the determination of isoelectric point for nanoparticles with different sizes. Sample 1: 37 nm, Sample 2: 52 nm and Sample 3: 65 nm.

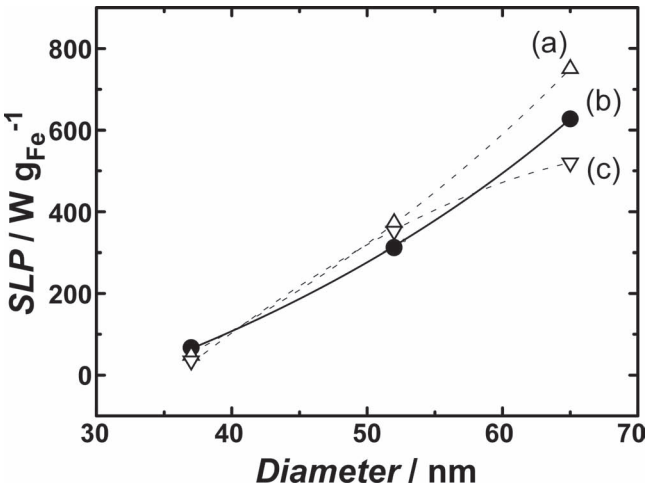

Figure 5. SLP correlation to the nanoparticle diameter for the concentrations 0.5 (a), 2 (b) and 4 mg_{Fe}/mL (c) measured at applied field intensity 300 Oe.

calculated to occur for roughly 30 nm diameter,[27] no distinct data to show this were obtained from magnetic measurements, neither in our recent quantum electronic transport experiments in individual Fe-MgO particles above 100 nm.[28] hinting the existence of uniaxial anisotropy despite their cubic crystal symmetry.[19] Consequently, for particles with such magnetic and morphological characteristics a heating mechanism through hysteresis losses is expected to dominate.

We find significant changes in the hyperthermia response depending on size and concentration, even though there are minimal differences in the features of the hysteresis loops. **Figure 5** indicates that the heating rate is proportional to the particle size; the bigger the particle, the higher the SLP. The trend of SLP increasing following the particle diameter is similar for all fluid concentrations in the range 0.5–4 mg_{Fe}/mL. The origin of this behavior is not yet fully apprehended, but two hypotheses can be put forward to explain it. Firstly, one could consider another relaxation mechanism contributing to the SLP besides the hysteresis losses, for instance the Brownian relaxation. Accordingly, a size-dependent effect has been previously demonstrated for iron oxide nanoparticles.[29] In fact, for monodisperse superparamagnetic samples it has been predicted that there would be an optimum particle size which would yield the highest heating rate for a given set of experimental conditions.[17] But the large mean particle diameters and frequencies discussed here do not seem to support this hypothesis.[30] Furthermore, particles have shown to retain their original hyperthermia activities even after cell internalization,[18] contrary to what would be expected for magnetic energy dissipation through Brown fluctuations.[16] Secondly, it might also happen that the observed features are a natural consequence of theories deriving from the Stoner–Wohlfarth model of single-domain particles well above the SPM regime. In a recent study B. Mehdaoui et al.[6] calculated the optimal diameter for maximizing the hysteresis losses, as a function of the applied field. We recognize striking similarity in our results with the theoretical curves published by B. Mehdaoui et al. (Figure 4 within the aforementioned work) though the optimal diameter is predicted to be 25–30 nm for the high magnetic field amplitude used in our case. We attribute the discrepancies between their numerical simulations and our experimental data to the presence of magnetic interactions in the samples, leading to an effective anisotropy constant differing from the one considered by B. Mehdaoui et al.

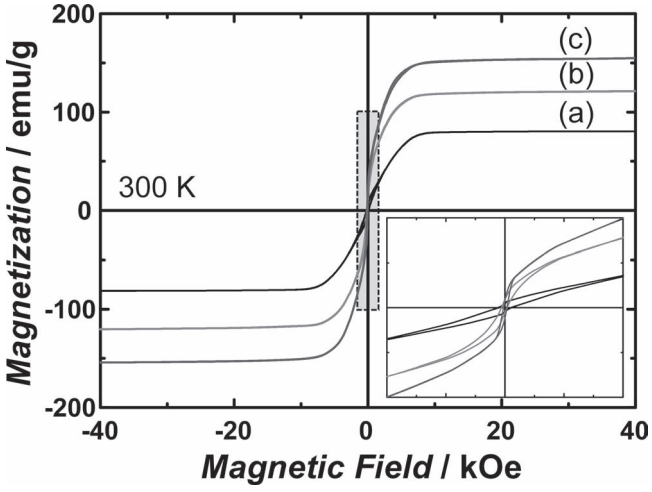

Figure 4. Room temperature hysteresis loops for Sample 1: 37 nm particles with 31% wt. Fe, (a), Sample 2: 52 nm with 53% wt. Fe (b) and Sample 3: 65 nm with 72% wt. Fe (c). The saturation magnetization is increased accordingly to the Fe content. Inset: Detail of hysteresis loops.

So far we have considered the tunability of the hyperthermia response with the diameter of the magnetic particles. Likewise, dipole-dipole interactions can be similarly tuned by particle volume fraction.[10] The volume fraction, defined here is the ratio between the volume occupied by the magnetic particles over the volume of the solution.

Apparently, the separation between particles is increasing against the particle volume fraction, either by increasing particle size or decreasing particle concentration.[31] It means

that, at constant concentration value, if the size of the particles is increased by a factor of two, the number of particles is reduced by a factor of eight, so the interparticle distances are analogously augmented. In a previous work, we have shown both experimental evidence and Monte Carlo modeling of the effects of interparticle dipolar interactions on the hysteresis losses.[19] Results indicate that SLP values decrease with concentration i.e. volume fraction, according to an increase in the dipolar field intensity.

This is also verified by Figure 5 for the larger particles; when concentration effect seems more pronounced and SLP values gradually decrease indicating the concentration hindering in the heating rate via dipolar interactions. (more SLP experimental data appear in the Supporting Information S.2 Section).

A similar qualitative behavior might be expected when increasing the particle volume fraction due to the formation of agglomerates. A broad size distribution virtually facilitates the building of compact clusters because small particles readily fill gaps between larger ones.[32] and SLP was observed to increase with particle packing fraction.[33] Contrary, in our case SLP was found to decrease with particle packing fraction while size-dependence of hysteresis losses resembles literature report of narrow size distribution behavior (see, for instance, Figure 8 in Reference [34].)

Thus, to evaluate the effect of nanoparticles' concentration and size on the hyperthermia, we compare the variation of SLP with fluid concentration (**Figure 6**). In all cases, at an applied field of 150 Oe the SLP follows a continuous increase that saturates at high concentrations. This AC field is much smaller than the saturation field (>5 kOe as indicated in Figure 4) so its application eventually leads to limited heating conversion due to recording of minor loops instead of fully saturated loops. This behavior has been analyzed in detail in a previous article.[19] Curiously enough, the heating rate under high intensity fields (300 Oe) increases with the concentration until it reaches a maximum value and then falls at highly concentrated fluids. The peak position stands at around 2 mg_{Fe}/mL for 37 nm particles (sample 1) but moves to lower concentrations for 52 nm (sample 2), while it is considered below 0.5 mg_{Fe}/mL for 65 nm (sample 3). This is probably determined by the mean particle size and the fluid concentration according to the competition of dipolar interactions and magnetic anisotropy.

To understand what causes this peculiar behavior of SLP, we performed numerical Monte Carlo simulations in the same way as in Ref. 19, i.e. calculating hysteresis cycles at different sample concentrations and evaluating the hysteresis loop area. This computational approach provides us with a reliable tool to study whether the non-monotonic SLP dependences on sample concentration and particle size displayed in Figure 6 can be attributed exclusively to dipolar interaction effects (and their interplay with anisotropy and thermal energies, together with particle size). For that purpose, a series of numerical simulations with the sample concentration (c) was performed. Different particles' characteristics (size (D), anisotropy constant-K and saturation magnetization-M_S) and temperature have been considered, aiming to cover different experimental conditions pertinent for magnetic hyperthermia (details about the characteristics of the particles and simulation procedure appear in the Supporting Information, S.3 Section). The strategy involved the definition of a dimensionless parameter $c_0 = 2K/M_S^2$, to

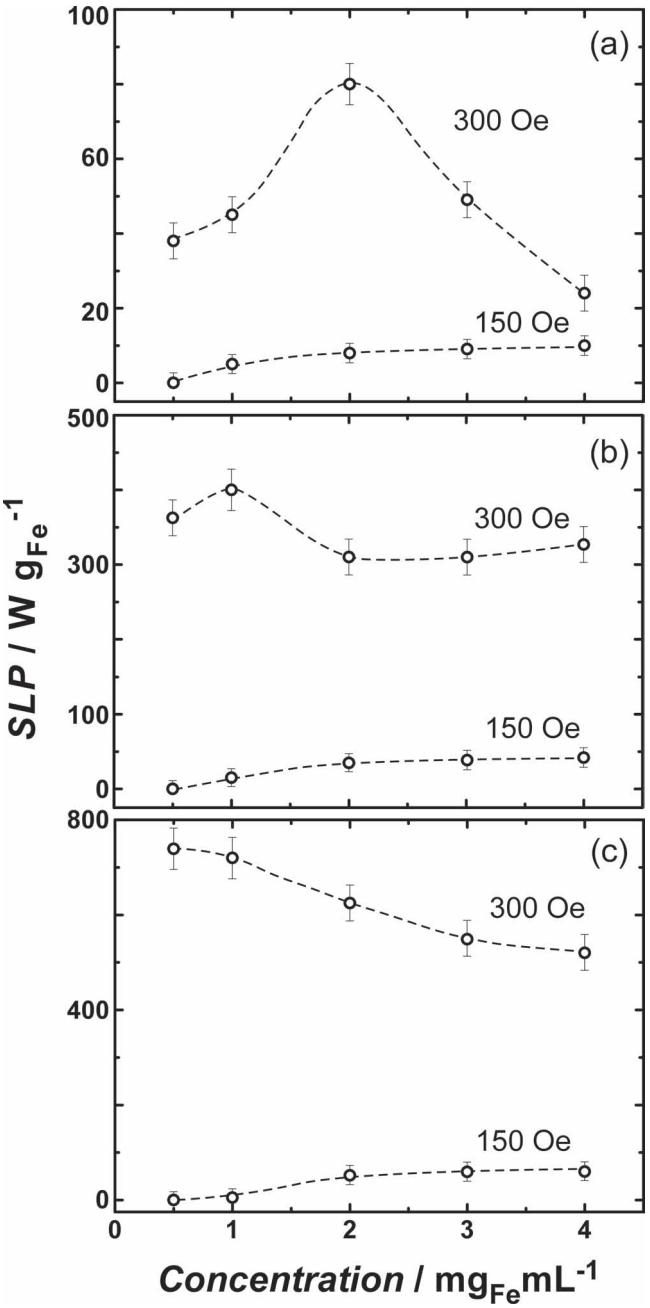

Figure 6. SLP dependence on the dispersion concentration for sample 1 of 37 nm particles (a), sample 2 of 52 nm particles (b) and sample 3 of 65 nm particles (c) measured at applied field intensities of 150 and 300 Oe. Connecting lines are guides to the eye.

describe the relative influence of the dipolar energy in comparison with the anisotropy one,[35] so that we directly correlate magneto-structural characteristics of the particles (K, M_S) to dipolar interaction effects.

In **Figure 7**(a) the hysteresis loop area deduced from the simulations is compared to the scaling factor c/c_0 weighting the dipolar energy to the sample concentration, for particles between 20 and 65 nm. Normalization by $2K$ accounts for the fact that hysteresis losses are (in first approximation, at very

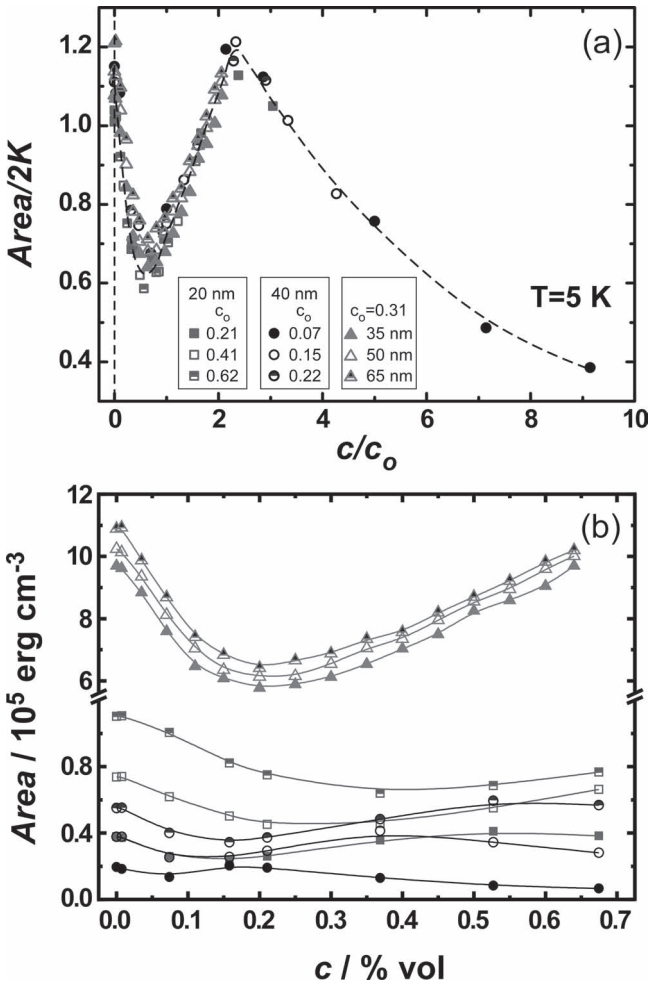

Figure 7. (a) Universal changes of the hysteresis area and its concentration dependence on magneto-structural parameters for particles well below the superparamagnetic transition. Data is presented for different types and sizes of particles (see legend: size was kept constant while varying $c_0 = 2K/M_S^2$; size was varied while keeping $c_0 = 0.31$). The lines connecting points are guides to the eye. (b) evolution of the hysteresis area *vs.* concentration in real units. Circles and squares might account for Fe_2O_3/Fe_3O_4 nanoparticles usually discussed in the literature, while full symbols account for Fe-MgO core-shell entities.

low temperature and for the non-interacting case) given by the anisotropy energy, twice its value for a full hysteresis cycle. Remarkably, data fall into a single universal curve at the low temperature of the simulations ($T = 5$ K). Furthermore, the several experimental trends of the SLP displayed in Figure 6 are in obvious agreement with partial ranges of this general curve, thus giving additional support to the role of c_0 as a general scaling parameter to describe dipole-dipole interacting systems. Thus, it is shown that the area of the hysteresis cycles (and consequently the coercive field) varies non-monotonically with the amplitude of the dipolar interactions. An example of the latter can be found in the elegantly-designed experiment of Kronast et al.[36] (see for instance Figure 2 within that paper).

Figure 7(b) displays the evolution of the hysteresis area with sample concentration for three Fe-MgO core-shell particles, with sizes of 35 nm, 50 nm, and 65 nm. In addition, in order to have a more accurate approach to the role played by the interparticle dipolar coupling we have also simulated the hysteresis properties of magnetic nanoparticles with very low magnetic anisotropy, which are more sensitive to the influence of the dipolar interaction energy. These particles have also much lower M_S values, of the order of typical of iron oxide nanoparticles, and smaller sizes, in order to cover a wide spectrum of magnetic nanoparticles parameters (see supporting information S.3 section for further details). It is observed that interparticle dipolar interactions can have a great influence on the heating performance of the particles, which follow apparently very dissimilar trends depending on their characteristics. It is worthy to note the large difference in the magnitude of the hysteresis losses for the different types of particles, above an order of magnitude smaller for the low anisotropy cases. Particularly, for the Fe-MgO particles, smaller sizes results in smaller hysteresis values, being this decrease attributable to the higher sensitivity to thermal energy. A more complex trend is observed at higher temperature as a result of the different influence of thermal excitations depending on the particle size and anisotropy energy (see Supporting information S.3 section). It is the subject of a future work to investigate the influence of temperature on the shape of this universal curve, as well as its dependence on the maximum applied field defining minor hysteresis cycles and the AC field frequency.

In summary, we have confirmed by means of a computational technique the idea that correlations arising from dipole-dipole interactions should cause a significant effect on the hyperthermia, obtaining a behavior in quantitative agreement with what is observed in experiment. Such an effect on the SLP, which results in low or high values depending on magnetic anisotropy, agglomeration, and particle size, can be visualized in a simple model: when the particles are sufficiently far apart one from the other (low packing fraction-diluted case), they can be considered as non-interacting magnetic entities, and the SLP increases with concentration up to the point when the magnetic interactions between particles become comparable to the anisotropy field. For larger packing fractions, the magnetic interactions increase substantially forcing a drop in the SLP. As such, our calculation represents an analytical model of hyperthermia in magnetic interacting-particle systems to explain in a simple way the ubiquitous behavior observed in this class of materials. Equally important, our results show that in order to optimize magnetic nanoparticle hyperthermia multiple parameters should be fine-tuned, though confirming that single-domain nanoparticles are the most efficient for biomedical applications. In particular, the universal curve predicts the existence of a specific value of concentration that optimizes the effect of the dipolar interactions. Obviously, further work is required before firm conclusions can be drawn, but it might happen magnetically coupled nanoparticles could be of help to improve hyperthermia efficiency as do in MRI imaging.[37]

2. Experimental Section

Synthesis of core/shell nanoparticles: Tuning the experimental conditions allowed us to produce samples of different sizes displaying

a magnetization close to the bulk value. In the studied samples, the chamber's pressure was set to 3 mbar. The targets used for Fe-MgO nanoparticles production were cold-pressed pellets prepared by mixing Fe and MgO powders, as well as an excess of Mg to inhibit iron oxidation. Fe powder was purchased from BASF (purity > 99.5%). MgO (99.998%) was purchased from Alfa Aesar. Mg (99.9%) was purchased from Sigma Aldrich. However, it should be apparent to those skilled in this methodology that they can readily change, for instance, the pressure and target composition in order to optimize further the above picture.

Structural and magnetic characterization: The detailed structural characterization of our samples was carried out by means of X-ray diffraction on a Rigaku powder diffractometer using Cu-K_a radiation. SEM images were obtained using a QUANTA FEI 200 instrument with a field-emission gun operating at 30 kV. For the TEM analysis, a drop of the colloidal solution in ethanol was deposited onto a thin carbon film supported by a copper TEM grid. Measurements were carried out with a Jeol JEM-1210 microscope at an acceleration voltage of 120 kV. The percentage of iron in nanopowders was determined by chemical analysis via graphite furnace atomic absorption spectrophotometry (Perkin Elmer Analyst 800) after diluting a weighted quantity in HCl. Quasistatic magnetic measurements were carried out on loosely packed powdered samples using a Quantum Design MPMS XL-7T SQUID magnetometer. The hysteresis loops were measured at 300 K.

Suspensions stability: Zeta-potential measurements were carried out to quantify the magnitude of the electrical charge at the double layer of nanoparticles surface and define the isoelectric point (IEP). A dispersion of nanoparticles in an electrolyte solution (0.01 M $NaNO_3$) was poured into the electrophoresis cell of a Rank Brothers Micro-electrophoresis Apparatus Mk II device and the electrophoretic velocity was recorded. The *pH* was adjusted at different *pH* values (5-13) by adding either HNO_3 or NaOH and left to equilibrate for 60 min under stirring.

Magnetically induced AC hyperthermia: Dispersions of 0.5–4 mg Fe/mL were prepared by the addition of nanopowders into distilled water and sonication for 10 min. A test tube containing 2 mL of the dispersion was placed in the center of a water-cooled induction coil with 23 mm diameter consisting of three turns, and connected to an AC field generator of 4.5 kW. The AC thermal response of the samples was measured at 765 kHz by recording the temperature rise with an OpSens PicoM optic fiber thermometer during ac field (between 150 and 300 Oe) application. The Specific Loss Power (SLP), which refers to the amount of energy converted into heat per time and mass of the magnetic nanoparticles, was calculated from the heat transfer equation [2].

Please note: Supporting Information Available: XRD patterns, and quantitative Rietveld analysis, of Fe-MgO nanoparticles prepared changing the target composition. Additional SLP measurements. Computational details.

Supporting Information

Supporting Information is available from the Wiley Online Library or from the author.

Acknowledgements

We thank the Centro de Supercomputación de Galicia (CESGA) for the computational facilities. This work was co-financed by the European Council's 7th Framework SFERA project No 228296, FEDER funds, Spanish MEC (MAT2006-13572-C02-01 and MAT2009-08165), CONSOLIDER (CSD2007-00041), Generalitat de Catalunya (2009SGR-00129), and Xunta de Galicia (INCITE 08PXIB236052PR). C. M. Boubeta and I. Conde-Leborán were supported by the "Ramón y Cajal" and FPI Spanish programs, respectively. K. Simeonidis acknowledges "Education and Lifelong Learning" Operational Program funded by EU-European Social Fund (ESF) and GSRT.

Received: February 1, 2012
Revised: March 22, 2012
Published online: May 11, 2012

[1] H. B. Na, I. C. Song, T. Hyeon, *Adv. Mater.* **2009**, *21*, 2133; and also J. D. G. Durán, J. L. Arias, V. Gallardo, A. V. Delgado, *J. Pharm. Sci.* **2008**, *97*, 2948.
[2] C. S. S. R. Kumar, F. Mohammad, *Adv. Drug Deliv. Rev.* **2011**, *63*, 789.
[3] C. Martinez-Boubeta, Ll. Balcells, R. Cristofol, C. Sanfeliu, E. Rodriguez, R. Weissleder, S. Lope-Piedrafita, K. Simeonidis, M. Angelakeris, F. Sandiumenge, A. Calleja, L. Casas, C. Monty, B. Martínez, *Nanomed. Nanotech. Biol. Med.* **2010**, *6*, 362.
[4] L.-M. Lacroix, N. F. Huls, D. Ho, X. Sun, K. Cheng, S. Sun, *Nano Lett.* **2011**, *11*, 1641.
[5] J.-H. Lee, J.-t. Jang, J.-s. Choi, S. H. Moon, S.-h. Noh, J.-w. Kim, J.-G. Kim, I.-S. Kim, K. I. Park, J. Cheon, *Nature Nanotech.* **2011**, *6*, 418.
[6] B. Mehdaoui, A. Meffre, J. Carrey, S. Lachaize, L.-M. Lacroix, M. Gougeon, B. Chaudret, M. Respaud, *Adv. Func. Mater.* **2011**, *21*, 4573.
[7] W. S. Seo, J. H. Lee, X. Sun, Y. Suzuki, D. Mann, Z. Liu, M. Terashima, P. C. Yang, M. V. McConnell, D. G. Nishimura, H. Dai, *Nat. Mater.* **2006**, *5*, 971.
[8] Y. H. Xu, J. P. Wang, *Appl. Phys. Lett.* **2007**, *91*, 233107.
[9] D. A. Bazylinski, R. B. Frankel, *Nature Rev.* **2004**, *2*, 217.
[10] K. Butter, P. H. H. Bomans, P. M. Frederik, G. J. Vroege, A. P. Philipse, *Nature Mater.* **2003**, *2*, 88.
[11] K. Nakata, Y. Hu, O. Uzun, O. Bakr, F. Stellacci, *Adv. Mater.* **2008**, *20*, 4294.
[12] J.-H. Park, G. von Maltzahn, L. Zhang, M. P. Schwartz, E. Ruoslahti, S. N. Bhatia, M. J. Sailor, *Adv Mater.* **2008**, *20*, 1630.
[13] R. Hergt, R. Hiergeist, M. Zeisberger, D. Schüler, U. Heyen, I. Hilger, W. A. Kaiser, *J. Magn. Magn. Mater.* **2005**, *293*, 80.
[14] A. Urtizberea, E. Natividad, A. Arizaga, M. Castro, A. Mediano, *J. Phys. Chem. C* **2010**, *114*, 4916.
[15] S. A. Majetich, T. Wen, R. A. Booth, *ACS Nano* **2011**, *5*, 6081.
[16] J.-P. Fortin, C. Wilhelm, J. Servais, C. Méneger, J.-C. Bacri, F. Gazeau, *J. Am. Chem. Soc.* **2007**, *129*, 2628.
[17] R. E. Rosensweig, J. Magn. *Magn. Mater.* **2002**, *252*, 370.
[18] R. Hergt, S. Dutz, M. Röder, *J. Phys.: Condens. Matter.* **2008**, *20*, 385214.
[19] A. Jordan, P. Wust, H. Fähling, W. John, A. Hinz, R. Felix, *Int. J. Hyperthermia* **2009**, *25*, 499.
[20] A. Chalkidou, K. Simeonidis, M. Angelakeris, T. Samaras, C. Martinez-Boubeta, Ll. Balcells, K. Papazisis, C. Dendrinou-Samara, O. Kalogirou, *J. Magn. Magn. Mater.* **2011**, *323*, 775.
[21] D. Serantes, D. Baldomir, C. Martinez-Boubeta, K. Simeonidis, M. Angelakeris, E. Natividad, M. Castro, A. Mediano, D. X. Chen, A. Sanchez, Ll. Balcells, B. Martinez, *J. Appl. Phys.* **2010**, *108*, 073918.
[22] S. Zhang, J. Li, G. Lykotrafitis, G. Bao, S. Suresh, *Adv. Mater.* **2009**, *21*, 419.
[23] J.-P. Fortin, F. Gazeau, C. Wilhelm, *Eur. Biophys. J.* **2008**, *37*, 223.
[24] C. Martinez-Boubeta, Ll. Balcells, S. Valencia, D. Schmitz, C. Monty, B. Martínez, *Appl. Phys. Lett.* **2009**, *94*, 262507.
[25] H. M. Rietveld, *J. Appl. Crystallogr.* **1969**, *2*, 65.

[26] M. Kosmulski, "*Chemical properties of material surfaces*", Marcel Dekker, New York **2001**.
[27] C. Chen, O. Kitakami, Y. Shimada, *J. Appl. Phys.* **1998**, *84*, 2184.
[28] C. Martinez-Boubeta, Ll. Balcells, C. Monty, P. Ordejon, B. Martínez, *Appl. Phys. Lett.* **2009**, *94*, 062507.
[29] M. Gonzales-Weimuller, M. Zeisberger, K. M. Krishnan, *J. Magn. Magn. Mater.* **2009**, *321*, 1947.
[30] N. A. Usov, *J. Appl. Phys.* **2010**, *107*, 123909.
[31] A. Wang, J. Li, R. Gao, *Appl. Phys. Lett.* **2009**, *94*, 212501.
[32] D. Eberbeck, J. Bläsing, *J. Appl. Cryst.* **1999**, *32*, 273.
[33] M. Jeun, S. Bae, A. Tomitaka, Y. Takemura, K. H. Park, S. H. Paek, K.-W. Chung, *Appl. Phys. Lett.* **2009**, *95*, 082501.
[34] R. Hergt, S. Dutz, M. Röder, *J. Phys.: Condens. Matter.* **2008**, *20*, 385214.
[35] D. V. Berkov, N. L. Gorn, P. Görnert, *J. Magn. Magn. Mater.* **2001**, *226*, 1936.
[36] F. Kronast, N. Friedenberger, K. Ollefs, S. Gliga, L. Tati-Bismaths, R. Thies, A. Ney, R. Weber, C. Hassel, F. M. Römer, A. V. Trunova, C. Wirtz, R. Hertel, H. A. Dürr, M. Farle, *Nano Lett.* **2011**, *11*, 1710.
[37] T.-J. Yoon, H. Lee, H. Shao, S. A. Hilderbrand, R. Weissleder, *Adv. Mater.* **2011**, *23*, 4793.